

Numerical method for inertial migration of particles in 3D channels

Laurent Chupin, Nicolae Cîndea*

Université Clermont Auvergne, Laboratoire de Mathématiques Blaise Pascal CNRS-UMR 6620, Campus des Cézeaux, F-63178 Aubière cedex, France

ARTICLE INFO

Article history:

Received 9 January 2019

Accepted 19 July 2019

Available online 23 August 2019

MSC:

35Q35

70-08

70E50

Keywords:

Fluid/particle

Inertial migration

Numerical method

Segré-Silberberg effect

Steady solutions

ABSTRACT

The aim of this paper is to propose a method to model and numerically simulate the inertial migration of particles in three-dimensional channels. The initial problem, coupling Navier–Stokes equations to the equations modeling the displacement of a spherical particle immersed in the fluid, is replaced by a first order expansion with respect to a small Reynolds number. We reduce the computation of the velocity of a spherical particle situated at a given position in a channel to the numerical solutions of several Stokes elementary problems. The proposed method is employed to numerically approach the steady solutions for different domain configurations.

© 2019 Published by Elsevier Ltd.

1. Introduction

Segré and Silberberg observed in 1960s that particles in suspension in a Poiseuille flow migrate, under the action of inertial forces, to an annular region having the same center as the circular section of the channel [16]. More recently, inertial migration of particles in microfluids was intensively studied in the perspective of very promising applications to micro-particles filtration and separation [17]. These applications use an early observation of Segré and Silberberg that different sized particles have different equilibrium regions, or, with other words, different focusing positions. While for channels of circular sections the equilibrium regions are well understood, for channels of less symmetric sections the situation is far from being clear, different experimental or numerical studies giving different numbers of equilibrium points in cases as simple as a channel with rectangular section [2–4,12,13].

The mathematical models for the inertial migration of particles in fluid flows have mostly been studied for channels with circular section. The radial symmetry of the section allows in that case to the simplification of the model by reducing the number of variables. Using the method of matched asymptotic expansions to model the disturbance of the flow due to the presence of a particle, at small Reynolds numbers, it is possible to compute the

equilibrium positions in circular channels [1,15]. More recently, a method based on the expansion of the solution of the fluid-particle problem with respect to the Reynolds number was proposed [8]. This method, formulated in a two-dimensional framework, allows the computation of the inertial equilibrium positions of a ball in a two dimensional channel for small Reynolds numbers by solving several stationary Stokes equations (the so-called *elementary problems*). The fact that there are only stationary Stokes problems to be solved is an advantage, from a computational perspective, with respect to other, more complex, approaches, such as directly solving Navier–Stokes equation coupled with a moving rigid structure [5,11].

The aim of the present work is to extend the method in [8] to a three-dimensional setting. More precisely, we reformulate the three-dimensional problem in order to emphasize a structure similar to the one obtained in the two dimensional framework and allowing the application of the ideas proposed in [8]. As in the two-dimensional case, for low Reynolds numbers, the computation of the inertial velocity of a spherical particle immersed in a three-dimensional fluid flowing in a channel is reduced to a small number of stationary Stokes problems. Even if numerically solving a Stokes equation is not very difficult, the presence of a high-number of unknowns in this case and the non-trivial geometry of the three-dimensional domain, require a finely-tuned numerical strategy. Particularly, we exploit the symmetry of the domain with respect to the plane orthogonal to the direction of the channel and containing the center of the ball, in order to reduce by half

* Corresponding author.

E-mail addresses: laurent.chupin@uca.fr (L. Chupin), nicolae.cindea@uca.fr (N. Cîndea).

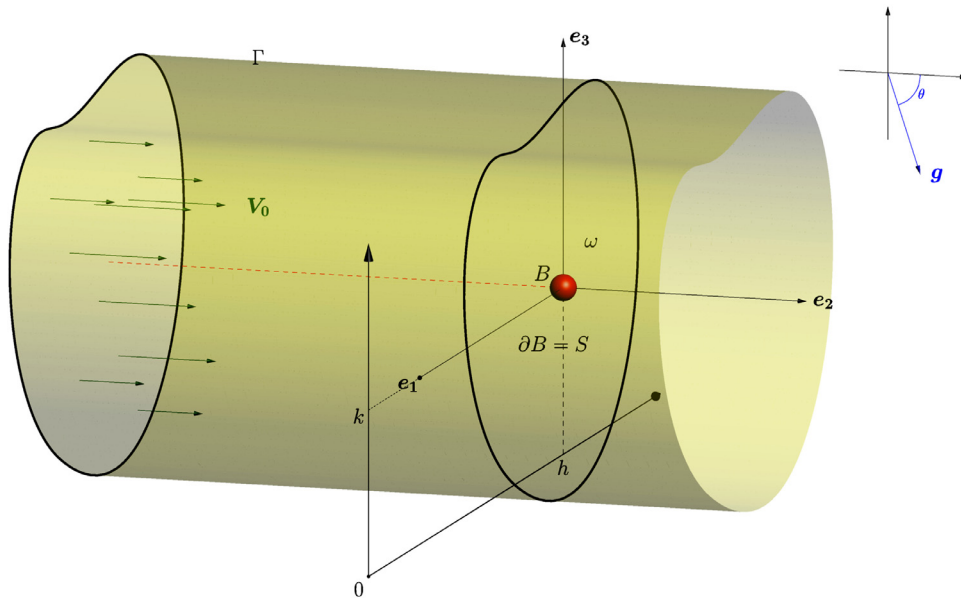


Fig. 1. Three-dimensional configuration.

the size of the problem. The mixed finite element method is employed to discretize the model on a non-uniform mesh which is much more refined on the surface of the ball than on the cylinder's walls. These features give a method which is fast enough to allow the analysis of a high number of geometrical configurations in an acceptable amount of time on a recent computer. We present in detail the development of the method, its implementation and we illustrate it for several channels with different sections. Afterwards, we validate the proposed method by comparing our numerical results to the well known results of Segré and Silberberg in a circular channel. More precisely, we obtain the same equilibrium positions just as in the physical experiments. The two situations were considered: when the gravity field is aligned to the channel's direction and when the gravity field forms a non-zero angle with the direction of the channel. Finally, we apply the method for other less symmetric geometries in order to investigate the inertial equilibrium positions of a particle immersed in a fluid flowing in such a cylinder. These numerical experiments were motivated by recent applications of the inertial migration of particles in a fluid to filtration and particle separation. The results we obtained are similar to some of the results in the recent literature and apparently contradicts other. Nevertheless, the observed disagreement could be explained by the fact that the proposed method is appropriate only for low Reynolds numbers.

The remaining part of the paper is structured as follows. In Section 2 we introduce the framework and we describe the model in detail. Section 3 introduce the *elementary problems* and study their properties. In Sections 4 and 5 we compute the inertial velocity of a particle placed in a Stokes flow and in a Navier-Stokes flow respectively (developed at the first order with respect to the Reynolds number). Finally, in Section 6 we propose a numerical method for the computation of the particle's inertial velocity and we numerically illustrate the method for different configurations. An important effort is employed to locate the steady solutions and the corresponding focusing positions.

2. Notation and description of the model

We consider a ball B immersed in a fluid which fills the interior of the cylinder $\omega \times \mathbb{R} \subset \mathbb{R}^3$. Each point of the bounded open domain $\omega \subset \mathbb{R}^2$ is parametrized by a pair of two reals so that the

position of the center of the ball is determined by its coordinates (h, k) (due to the invariance with respect to the direction of the cylinder, the last coordinate is useless). In practice, any coordinate system can be used. For example, polar coordinates are appropriate in the case of a disk, and Cartesian coordinates are better suited when ω is a rectangle.

We write the equations modeling this situation in a frame adapted to the configuration described above. We then introduce the orthonormal frame $(O, \mathbf{e}_1, \mathbf{e}_2, \mathbf{e}_3)$ as follows (see Fig. 1):

- the origin O coincides with the center of the ball B ,
- the direction of \mathbf{e}_2 corresponds to the direction of the cylinder,
- the plane $O\mathbf{e}_2\mathbf{e}_3$ generated by the vectors \mathbf{e}_2 and \mathbf{e}_3 contains the gravity field.

In this frame, the ball B of radius $R > 0$ is defined by

$$B = \{\mathbf{x} = (x, y, z) \in \mathbb{R}^3 : x^2 + y^2 + z^2 < R^2\}.$$

Its boundary is denoted by $\partial B = S$ and its outward unitary normal is denoted by \mathbf{n} .

Thus, the orientation of the cylinder with respect to the vertical position will be given according to an angle θ : if $\theta = 0$ then the axis of the cylinder is assumed to be vertical (aligned with the gravity vector), if $\theta = \frac{\pi}{2}$ then the axis of the cylinder is horizontal. The intermediate values of $\theta \in]0, \frac{\pi}{2}[$ make it possible to obtain any configuration. More precisely, the gravity force may be written as $\mathbf{g} = (0, g \cos \theta, -g \sin \theta)$.

The fluid domain corresponds to $\Omega = (\omega \times \mathbb{R}) \setminus \bar{B}$ whereas its lateral boundary is denoted by $\Gamma = \partial\omega \times \mathbb{R}$. It is important to note that this domain Ω should be labeled $\Omega_{h,k}$ since the position of the ball B with respect to the lateral boundary Γ depends on the parameters h and k .

In what follows, we are particularly interested in steady motions of the fluid-structure system described above, that is, the situations where the translational velocity \mathbf{U} and the angular velocity ω of the ball are constant in time, and the motion of the fluid as seen from a frame attached to the ball and moving with velocity \mathbf{U} is independent of time. The fluid flow is also an unknown of the problem so we aim to determine the velocity \mathbf{v} of the fluid as well as its pressure p .

Mathematically, our problem can be formulated as follows. Find $((\mathbf{v}, p), (\mathbf{U}, \boldsymbol{\omega}), (h, k))$ satisfying the equations

$$\begin{cases} \operatorname{div} \boldsymbol{\sigma} = \rho_f \mathbf{v} \cdot \nabla \mathbf{v}, & \operatorname{div} \mathbf{v} = 0, & \boldsymbol{\sigma} = 2\mu_f D\mathbf{v} - p \mathbf{Id} & \text{in } \Omega, \\ \mathbf{v}|_{\Gamma} = -\mathbf{U}, & \mathbf{v}|_S = \boldsymbol{\omega} \times \mathbf{x}, \\ \lim_{|y| \rightarrow +\infty} (\mathbf{v}(x, y, z) - V_0(x, z)\mathbf{e}_2) = -\mathbf{U} & \text{for all } (x, z) \in \omega, \\ \int_S \boldsymbol{\sigma} \cdot \mathbf{n} \, ds(\mathbf{x}) = -mg, & \int_S \mathbf{x} \times \boldsymbol{\sigma} \cdot \mathbf{n} \, ds(\mathbf{x}) = \mathbf{0}. \end{cases} \quad (1)$$

The three relationships in the first line of this system correspond to the momentum conservation of the fluid, the mass conservation of the fluid (reduced to a divergence free relation since we assume that the fluid is incompressible) and the Newtonian constitutive assumption elucidating the stress $\boldsymbol{\sigma}$ with respect to the velocity and the pressure, respectively. The physical constants ρ_f and μ_f correspond to the fluid density and the fluid viscosity, respectively. It should also be noted that forces due to gravity are not directly present in the conservation balance. In fact, they were integrated into the pressure term by writing $\mathbf{g} = \nabla \tilde{p}$ with $\tilde{p}(x, y, z) = g \cos(\theta)y - g \sin(\theta)z$.

The second and the third lines of the system (1) correspond to the boundary conditions imposed on the velocity field. These are Dirichlet-like conditions knowing that the model is written in a \mathbf{U} -velocity translation frame: we assume adherence on the ball and on the lateral walls. The condition at the infinite ends of the cylinder is given by a Poiseuille-type condition corresponding to a flow without the ball. More precisely, a flow in the cylinder $\omega \times \mathbb{R}$, satisfying the Navier-Stokes equation with homogeneous Dirichlet boundary condition (on Γ) has velocity and pressure fields given by:

$$\mathbf{v}_0(x, y, z) = V_0(x, z)\mathbf{e}_2, \quad p_0(x, y, z) = P_0(y) + g \cos(\theta)y - g \sin(\theta)z, \quad (2)$$

where V_0 is the solution of the elliptic problem

$$\begin{cases} -\Delta_{x,z} V_0 = \gamma & \text{in } \omega, \\ V_0|_{\partial\omega} = 0, \end{cases} \quad (3)$$

and where P_0 is given by $P_0(y) = \gamma y$. The constant γ is evaluated so that the flux $\int_{\omega} V_0 \, dx dz$ corresponds to an imposed value Φ .

The two last equalities in system (1) express the equilibrium of the particle (force and momentum). The two external forces acting on the particle being due to the gravity and to the buoyancy, we introduce the quantity m depending on the difference between the solid density ρ_s and the fluid density ρ_f : $m = \frac{4}{3}\pi R^3(\rho_s - \rho_f)$.

In order to write a model in a dimensionless form, we introduce the following changes of variables and of unknowns:

$$\begin{aligned} \mathbf{x} &= L\mathbf{x}^*, & \mathbf{v} &= V\mathbf{v}^*, & \boldsymbol{\sigma} &= \frac{\mu_f V}{L}\boldsymbol{\sigma}^*, & p &= \frac{\mu_f V}{L}p^*, & \mathbf{U} &= V\mathbf{U}^*, \\ \boldsymbol{\omega} &= \frac{V}{L}\boldsymbol{\omega}^*, & R &= LR^*, & V_0 &= \frac{\Phi}{L^2}V_0^*, \end{aligned}$$

where L is the characteristic length of the domain ω and $V = \sqrt{gR}$ is the reference velocity. The system (1) becomes the following dimensionless system (for simplicity all the stars (\star) appearing as upper indices are omitted):

$$\begin{cases} \operatorname{div} \boldsymbol{\sigma} = \operatorname{Re} \mathbf{v} \cdot \nabla \mathbf{v}, & \operatorname{div} \mathbf{v} = 0, & \boldsymbol{\sigma} = 2D\mathbf{v} - p \mathbf{Id} & \text{in } \Omega, \\ \mathbf{v}|_{\Gamma} = -\mathbf{U}, & \mathbf{v}|_S = \boldsymbol{\omega} \times \mathbf{x}, \\ \lim_{|y| \rightarrow +\infty} (\mathbf{v}(x, y, z) - V_0(x, z)\mathbf{e}_2) = -\mathbf{U} & \text{for all } (x, z) \in \omega, \\ \int_S \boldsymbol{\sigma} \cdot \mathbf{n} \, ds(\mathbf{x}) = \mathcal{G}a \operatorname{Re} (\cos(\theta)\mathbf{e}_2 + \sin(\theta)\mathbf{e}_3), \\ \int_S \mathbf{x} \times \boldsymbol{\sigma} \cdot \mathbf{n} \, ds(\mathbf{x}) = \mathbf{0}. \end{cases} \quad (4)$$

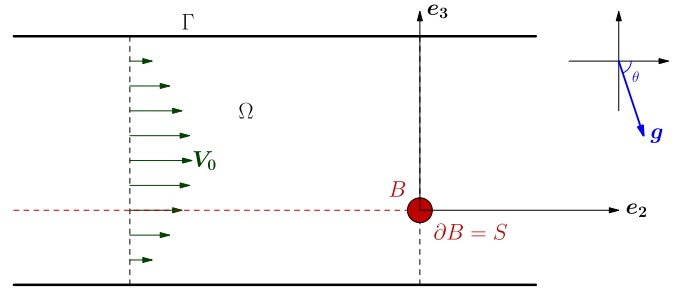


Fig. 2. Two dimensional configuration.

The scalar velocity V_0 appearing in the third equation of system (4) is the unique solution to

$$\Delta_{x,z} V_0 = c \quad \text{on } \omega, \quad \int_{\omega} V_0 \, dx dz = \mathcal{F}r, \quad V_0|_{\partial\omega} = 0,$$

where c is a constant. Obviously, in the system (4), we have $\Omega = (\omega \times \mathbb{R}) \setminus \bar{B}$ where $\omega \subset \mathbb{R}^2$ is a bounded domain of characteristic size 1 and where B is the ball centered in $(0,0,0)$ and with radius $\frac{R}{L}$. The dimensionless numbers Re , $\mathcal{F}r$ and $\mathcal{G}a$ correspond to the Reynolds number, the Froude number and to the Gravity number respectively. They are defined from physical quantities characterizing the situation:

$$\operatorname{Re} = \frac{\rho_f V L}{\mu_f}, \quad \mathcal{F}r = \frac{\Phi}{L^2 V} \quad \text{and} \quad \mathcal{G}a = \frac{4\pi}{3} \left(\frac{R}{L}\right)^2 \left(\frac{\rho_s}{\rho_f} - 1\right). \quad (5)$$

Remark 2.1 (2D). The three-dimensional model generalizes the two-dimensional setting described in Fig. 2. In the two-dimensional case, the variable x is not present and the position vector is given by $\mathbf{x} = (y, z)$. The flow (\mathbf{v}_0, P_0) corresponds to the usual Poiseuille flow in a channel.

Remark 2.2 (Slip boundary condition). We can consider the case where slip is allowed at the fluid/solid interface, through a Navier condition. This consists in rewriting the boundary condition $\mathbf{v}|_S = \boldsymbol{\omega} \times \mathbf{x}$ as follows:

$$\mathbf{v} \cdot \mathbf{n} = 0 \quad \text{and} \quad \mathbf{v} + \xi \mathbf{n} \times (\boldsymbol{\sigma} \cdot \mathbf{n}) \times \mathbf{n} = \boldsymbol{\omega} \times \mathbf{x}. \quad (6)$$

In other words, only the normal component of the relative velocity of the fluid is zero, to ensure impermeability. The tangential components are non-zero, and are proportional to the stress constraint, with constant slip length $\xi > 0$. In the same way, it is also possible to consider slip on the lateral boundary Γ .

System (4) is in fact the stationary case of an evolutionary model. The boundary condition $\mathbf{v}|_{\Gamma} = -\mathbf{U}$ must involve a non-penetration condition. Given the shape of the domain (a cylinder), this condition implies that a physical steady solution must satisfy $\mathbf{U}_1 = \mathbf{0}$ and $\mathbf{U}_3 = \mathbf{0}$. We then give the following definition:

Definition 2.1. We call a steady solution to system (4) any solution $((\mathbf{v}, p), \mathbf{U}, \boldsymbol{\omega})$ such that $\mathbf{U}_1 = \mathbf{U}_3 = \mathbf{0}$.

3. Study of elementary problems

The construction of the solution for problem (4) is based on the use of the so called *elementary problems*. More precisely, we will

consider the following Stokes problems, for $i \in \{1, 2, \dots, 6\}$:

$$\begin{cases} \operatorname{div} \boldsymbol{\sigma}^{(i)} = \mathbf{0}, & \operatorname{div} \mathbf{v}^{(i)} = \mathbf{0}, & \boldsymbol{\sigma}^{(i)} = 2D\mathbf{v}^{(i)} - p^{(i)} \mathbf{Id} & \text{in } \Omega, \\ \mathbf{v}^{(i)}|_{\Gamma} = \mathbf{0}, & \mathbf{v}^{(i)}|_S = \boldsymbol{\beta}_i, \\ \lim_{|y| \rightarrow +\infty} \mathbf{v}^{(i)}(x, y, z) = \mathbf{0} & \text{for all } (x, z) \in \omega, \end{cases} \quad (7)$$

where $\boldsymbol{\beta}_i = \mathbf{e}_i$ for $i \in \{1, 2, 3\}$ and $\boldsymbol{\beta}_i = \mathbf{e}_{i-3} \times \mathbf{x}$ for $i \in \{4, 5, 6\}$.

The existence and uniqueness of the regular solutions $(\mathbf{v}^{(i)}, p^{(i)})$ of (7) is classical.

Remark 3.1. Note that every couple $(\mathbf{v}^{(i)}, p^{(i)})$ depends on the parameters (h, k) only through the definition of the fluid domain Ω . Furthermore, $\mathbf{v}^{(i)}, p^{(i)}$ and all their derivatives decay exponentially fast to zero as $|y| \rightarrow +\infty$, see [6, Chap. XI]. From a numerical point of view, it is therefore reasonable to solve these linear problems in a bounded domain given by $\Omega_M = \Omega \cap \{(x, y, z) \in \mathbb{R}^3; -M < y < M\}$, for M large enough.

Proposition 3.1. The matrix $\mathcal{A} \in \mathcal{M}_{6,6}(\mathbb{R})$ defined by

$$A_{ij} = \int_S (\boldsymbol{\sigma}^{(i)} \cdot \mathbf{n}) \cdot \boldsymbol{\beta}_j \, ds(\mathbf{x}), \quad 1 \leq i, j \leq 6$$

is symmetric. Moreover, half of its coefficients are zero and the structure of this matrix is given by

$$\mathcal{A} = \begin{pmatrix} A_{11} & 0 & A_{13} & 0 & A_{15} & 0 \\ 0 & A_{22} & 0 & A_{24} & 0 & A_{26} \\ A_{31} & 0 & A_{33} & 0 & A_{35} & 0 \\ 0 & A_{42} & 0 & A_{44} & 0 & A_{46} \\ A_{51} & 0 & A_{53} & 0 & A_{55} & 0 \\ 0 & A_{62} & 0 & A_{64} & 0 & A_{66} \end{pmatrix}.$$

The matrices obtained by keeping only the even rows and columns and by keeping the odd rows and columns, respectively, denoted by

$$\mathcal{A}_I = \begin{pmatrix} A_{11} & A_{13} & A_{15} \\ A_{31} & A_{33} & A_{35} \\ A_{51} & A_{53} & A_{55} \end{pmatrix} \quad \text{and} \quad \mathcal{A}_P = \begin{pmatrix} A_{22} & A_{24} & A_{26} \\ A_{42} & A_{44} & A_{46} \\ A_{62} & A_{64} & A_{66} \end{pmatrix}$$

are invertible.

Proof. Multiplying the first equation of (7) by $v^{(j)}$ and integrating by parts, we deduce that

$$A_{ij} = 2 \int_{\Omega} D\mathbf{v}^{(i)} : D\mathbf{v}^{(j)} \, d\mathbf{x}.$$

The symmetry immediately follows.

The cancellation of certain coefficients is a consequence of the parity of the solutions with respect to the variable y . For instance, the components $v_1^{(1)}$ and $v_3^{(1)}$ are even (with respect to y), as well as the pressure $p^{(1)}$, whereas $v_2^{(1)}$ is odd. We deduce that the components $\sigma_{11}^{(1)}, \sigma_{22}^{(1)}, \sigma_{33}^{(1)}, \sigma_{13}^{(1)}$ and $\sigma_{31}^{(1)}$ are even. Thus $(\boldsymbol{\sigma}^{(1)} \cdot \mathbf{n}) \cdot \mathbf{e}_2$ is odd: its integral over S is zero, that is $A_{12} = 0$.

To prove the invertibility of matrices \mathcal{A}_I and \mathcal{A}_P , we proceed as follows: let $\widehat{\mathbf{v}} = \sum_i \lambda_i \mathbf{v}^{(i)}$ and $\widehat{p} = \sum_i \lambda_i p^{(i)}$. By linearity, $(\widehat{\mathbf{v}}, \widehat{p})$ satisfies a Stokes system. Multiplying this Stokes equation by $\widehat{\mathbf{v}}$ and integrating by parts, we obtain

$$\sum_{i,j} \lambda_i \lambda_j A_{ij} = 2 \int_{\Omega} |D\widehat{\mathbf{v}}|^2 \, d\mathbf{x} \geq 0.$$

Taking $\lambda_2 = \lambda_4 = \lambda_6 = 0$, we obtain that the quadratic form associated to the matrix \mathcal{A}_I is positive definite, and thus that \mathcal{A}_I is invertible. Similarly, if we take $\lambda_1 = \lambda_3 = \lambda_5 = 0$ we deduce that \mathcal{A}_P is invertible. \square

In order to find the conditions at infinity, we define $(\mathbf{v}^{(\infty)}, p^{(\infty)})$ the unique solution of the following problem:

$$\begin{cases} \operatorname{div} \boldsymbol{\sigma}^{(\infty)} = \mathbf{0}, & \operatorname{div} \mathbf{v}^{(\infty)} = \mathbf{0}, & \boldsymbol{\sigma}^{(\infty)} = 2D\mathbf{v}^{(\infty)} - p^{(\infty)} \mathbf{Id} & \text{in } \Omega, \\ \mathbf{v}^{(\infty)}|_{\Gamma} = \mathbf{0}, & \mathbf{v}^{(\infty)}|_S = \mathbf{0}, \\ \lim_{|y| \rightarrow +\infty} (\mathbf{v}^{(\infty)}(x, y, z) - V_0(x, z) \mathbf{e}_2) = \mathbf{0} & \text{for all } (x, z) \in \omega. \end{cases} \quad (8)$$

Remark 3.2. In the two dimensional situation, only vectors $\mathbf{v}^{(2)}, \mathbf{v}^{(3)}, \mathbf{v}^{(4)}$ and $\mathbf{v}^{(\infty)}$ are relevant and the matrices \mathcal{A}_I and \mathcal{A}_P become

$$\mathcal{A}_I^{(2d)} = (A_{33}) \quad \text{and} \quad \mathcal{A}_P^{(2d)} = \begin{pmatrix} A_{22} & A_{24} \\ A_{42} & A_{44} \end{pmatrix}.$$

Remark 3.3 (Slip boundary condition). If the slip boundary conditions are considered at the fluid/solid interface (see Remark 2.2), the boundary condition $\mathbf{v}^{(i)}|_S = \boldsymbol{\beta}_i$ in system (7) becomes

$$\mathbf{v}^{(i)} \cdot \mathbf{n} = 0 \quad \text{and} \quad \mathbf{v}^{(i)} + \xi \mathbf{n} \times (\boldsymbol{\sigma}^{(i)} \cdot \mathbf{n}) \times \mathbf{n} = \boldsymbol{\beta}_i. \quad (9)$$

Proposition 3.1 remains also true also in this case. Indeed, we have

$$A_{ij} = 2 \int_{\Omega} D\mathbf{v}^{(i)} : D\mathbf{v}^{(j)} \, d\mathbf{x} + \xi \int_S ((\boldsymbol{\sigma}^{(i)} \cdot \mathbf{n}) \cdot \mathbf{n}) ((\boldsymbol{\sigma}^{(j)} \cdot \mathbf{n}) \cdot \mathbf{n}) \, ds(\mathbf{x}).$$

Remark 3.4. Taking into account the symmetry of the domain (with respect to the plane $O\mathbf{e}_1\mathbf{e}_3$), we can evaluate the coefficients A_{ij} using only the values of the solutions of (7), for $i \in \{1, 2, \dots, 6\}$ in the half domain Ω_+ :

$$A_{ij} = 4 \int_{\Omega_+} D\mathbf{v}^{(i)} : D\mathbf{v}^{(j)} \, d\mathbf{x}, \quad (10)$$

where

$$\Omega^+ = \{(x, y, z) \in \Omega; y > 0\}.$$

Since it is sufficient to consider the elementary problems on the half domain Ω^+ , this remark is useful for the numerical implementation of the proposed method. We therefore divide by two the size of the linear system to solve.

4. Steady solutions and Stokes flow

This section is devoted to a preliminary study of the Stokes flow, formally obtained by setting $\mathcal{R}e = 0$ in (4). More precisely, we consider the following Stokes system:

$$\begin{cases} \operatorname{div} \boldsymbol{\sigma}_S = \mathbf{0}, & \operatorname{div} \mathbf{v}_S = \mathbf{0}, & \boldsymbol{\sigma}_S = 2D\mathbf{v}_S - p_S \mathbf{Id} & \text{in } \Omega, \\ \mathbf{v}_S|_{\Gamma} = -\mathbf{U}_S, & \mathbf{v}_S|_S = \boldsymbol{\omega}_S \times \mathbf{x}, \\ \lim_{|y| \rightarrow +\infty} (\mathbf{v}_S(x, y, z) - V_0(x, z) \mathbf{e}_2) = -\mathbf{U}_S & \text{for all } (x, z) \in \omega, \\ \int_S \boldsymbol{\sigma}_S \cdot \mathbf{n} \, ds(\mathbf{x}) = \mathbf{0}, & \int_S \mathbf{x} \times \boldsymbol{\sigma}_S \cdot \mathbf{n} \, ds(\mathbf{x}) = \mathbf{0}. \end{cases} \quad (11)$$

For any (h, k) , we explicitly determine a solution to this problem as a linear combination of solutions to the elementary problems (7). For this purpose, given $(\mathbf{U}_S, \boldsymbol{\omega}_S) \in \mathbb{R}^3 \times \mathbb{R}^3$, we consider the solution (\mathbf{v}_S, p_S) to the first three lines in (11). Multiplying the first equation of (11) by $\mathbf{v}^{(i)}$ and integrating by parts, we obtain that for every $i \in \{1, 2, \dots, 6\}$ we have

$$2 \int_{\Omega} D\mathbf{v}_S : D\mathbf{v}^{(i)} \, d\mathbf{x} = \int_S (\boldsymbol{\sigma}_S \cdot \mathbf{n}) \cdot \boldsymbol{\beta}_i \, ds(\mathbf{x}). \quad (12)$$

Given the definition of the vectors $\boldsymbol{\beta}_i$, the last two conditions of system (11) are fulfilled if and only if, for every $i \in \{1, 2, \dots, 6\}$ we have

$$\int_{\Omega} D\mathbf{v}_S : D\mathbf{v}^{(i)} \, d\mathbf{x} = 0. \quad (13)$$

Moreover, multiplying the first equation of (7) by $\mathbf{v}_S - V_0 \mathbf{e}_2 + \mathbf{U}_S$, we get:

$$2 \int_{\Omega} D\mathbf{v}_S : D\mathbf{v}^{(i)} \, d\mathbf{x} = \int_S (\boldsymbol{\sigma}^{(i)} \cdot \mathbf{n}) \cdot (\boldsymbol{\omega}_S \times \mathbf{x} - V_0 \mathbf{e}_2 + \mathbf{U}_S) \, ds(\mathbf{x}) + 2 \int_{\Omega} D(V_0 \mathbf{e}_2) : D\mathbf{v}^{(i)} \, d\mathbf{x} \tag{14}$$

Finally, the last two conditions of system (11) are equivalent to choose $(\mathbf{U}_S, \boldsymbol{\omega}_S) \in \mathbb{R}^3 \times \mathbb{R}^3$ such that for every $i \in \{1, 2, \dots, 6\}$ the following equality is verified:

$$\int_S (\boldsymbol{\sigma}^{(i)} \cdot \mathbf{n}) \cdot \mathbf{U}_S \, ds(\mathbf{x}) + \int_S (\mathbf{x} \times \boldsymbol{\sigma}^{(i)} \cdot \mathbf{n}) \cdot \boldsymbol{\omega}_S \, ds(\mathbf{x}) = \int_S (\boldsymbol{\sigma}^{(i)} \cdot \mathbf{n}) \cdot \mathbf{v}_0 \, ds(\mathbf{x}) - 2 \int_{\Omega} D(V_0 \mathbf{e}_2) : D\mathbf{v}^{(i)} \, d\mathbf{x} \tag{15}$$

These six linear equations can be put in a matrix form using the matrix \mathcal{A} introduced in the previous section:

$$\mathcal{A} \begin{pmatrix} U_1 \\ U_2 \\ U_3 \\ \omega_1 \\ \omega_2 \\ \omega_3 \end{pmatrix} = \begin{pmatrix} b_1 \\ b_2 \\ b_3 \\ b_4 \\ b_5 \\ b_6 \end{pmatrix}, \tag{16}$$

where, for any $i \in \{1, 2, \dots, 6\}$ the right-hand side of the equality is given by:

$$b_i = \int_S (\boldsymbol{\sigma}^{(i)} \cdot \mathbf{n}) \cdot \mathbf{v}_0 \, ds(\mathbf{x}) - 2 \int_{\Omega} D(V_0 \mathbf{e}_2) : D\mathbf{v}^{(i)} \, d\mathbf{x} \tag{17}$$

A symmetry with respect to the variable y argument shows that $b_1 = b_3 = b_5 = 0$ (see the proof of the Proposition 3.1 for similar computations). Thus, by rearranging the system (16), it can be written as:

$$\mathcal{A}_I \begin{pmatrix} U_1 \\ U_3 \\ \omega_2 \end{pmatrix} = \begin{pmatrix} 0 \\ 0 \\ 0 \end{pmatrix} \quad \text{and} \quad \mathcal{A}_P \begin{pmatrix} U_2 \\ \omega_1 \\ \omega_3 \end{pmatrix} = \begin{pmatrix} b_2 \\ b_4 \\ b_6 \end{pmatrix}. \tag{18}$$

Matrices $\mathcal{A}_I, \mathcal{A}_P$ being invertible, we deduce that the velocity \mathbf{U}_S will have only one non-zero component (the component U_2), and that it could be expressed using the solution of a linear system. In conclusion, we can state the following result:

Theorem 4.1. *For any parameters (h, k) , there exists a unique steady solution $(\mathbf{v}_S, p_S, \mathbf{U}_S, \boldsymbol{\omega}_S)$ to the system (11). This solution is explicitly given by*

$$\begin{aligned} \mathbf{v}_S &= U_2 \mathbf{v}^{(2)} + \omega_1 \mathbf{v}^{(4)} + \omega_3 \mathbf{v}^{(6)} + \mathbf{v}^{(\infty)} - U_2 \mathbf{e}_2, \\ p_S &= U_2 p^{(2)} + \omega_1 p^{(4)} + \omega_3 p^{(6)} + p^{(\infty)}, \\ \mathbf{U}_S &= U_2 \mathbf{e}_2, \end{aligned} \tag{19}$$

$$\boldsymbol{\omega}_S = \omega_1 \mathbf{e}_1 + \omega_3 \mathbf{e}_3,$$

where $(\mathbf{v}^{(i)}, p^{(i)})$, $i \in \{1, 2, \dots, 6\}$, (resp. $(\mathbf{v}^{(\infty)}, p^{(\infty)})$) are the solutions of the elementary Stokes problems (7) (resp. (8)), and where $(U_2, \omega_1, \omega_3)$ is the unique solution to $\mathcal{A}_P X = \mathbf{b}$, the matrix \mathcal{A}_P and the source term \mathbf{b} being respectively given in Proposition 3.1 and by (17).

Proof. It is enough to verify that the proposed solution is indeed adapted and verifies all the relationships in system (11). The uniqueness directly follows from the linearity of the Stokes equations. \square

Remark 4.1. For the two-dimensional case we obtain that for any $h \in \omega$, there exists a unique solution $(\mathbf{v}_S, p_S, \mathbf{U}_S, \boldsymbol{\omega}_S)$ to the system (11). This solution is explicitly given by

$$\begin{aligned} \mathbf{v}_S &= U_2 \mathbf{v}^{(2)} + \omega_1 \mathbf{v}^{(4)} + \mathbf{v}^{(\infty)} - U_2 \mathbf{e}_2, \\ p_S &= U_2 p^{(2)} + \omega_1 p^{(4)} + p^{(\infty)}, \\ \mathbf{U}_S &= U_2 \mathbf{e}_2, \\ \boldsymbol{\omega}_S &= \omega_1 \mathbf{e}_1, \end{aligned} \tag{20}$$

where $(U_2, \omega_1, 0)$ is the unique solution to $\mathcal{A}_P^{(2d)} X = \mathbf{b}^{(2d)}$, the matrix $\mathcal{A}_P^{(2d)}$ and the source term $\mathbf{b}^{(2d)}$ being respectively given in Remark 3.2 and by (17) by taking $i = 2, 4$.

5. Steady solutions for flows governed by Navier–Stokes equation

From Galdi [7, Th 3.4, page 252], we know that there is only one solution to the problem (4) when the Reynolds number $\mathcal{R}e$ is assumed to be small. Moreover, we know that this solution is continuous with respect to the Reynolds number:

$$\mathbf{v} = \mathbf{v}_S + \mathcal{O}_0(\mathcal{R}e),$$

where the velocity \mathbf{v}_S corresponds to the solution for the Stokes system (that is, the solution obtained in the previous section, see Theorem 4.1).

Multiplying the first equation of the system (4) by the elementary velocity fields $\mathbf{v}^{(i)}$, we proceed as in the beginning of the previous section and we obtain the relations

$$2 \int_{\Omega} D\mathbf{v} : D\mathbf{v}^{(i)} \, d\mathbf{x} + \mathcal{R}e \int_{\Omega} (\mathbf{v} \cdot \nabla \mathbf{v}) \cdot \mathbf{v}^{(i)} \, d\mathbf{x} = \int_S (\boldsymbol{\sigma} \cdot \mathbf{n}) \cdot \boldsymbol{\beta}_i \, ds(\mathbf{x}). \tag{21}$$

Following the same strategy as in the Stokes case, the solution of the system (4) satisfies

$$\mathcal{A}_I \begin{pmatrix} U_1 \\ U_3 \\ \omega_2 \end{pmatrix} = -\mathcal{R}e \begin{pmatrix} c_1 \\ c_3 \\ c_5 \end{pmatrix} - \mathcal{G}a \mathcal{R}e \begin{pmatrix} 0 \\ \sin \theta \\ 0 \end{pmatrix} + \mathcal{O}_0(\mathcal{R}e^2) \tag{22}$$

and

$$\mathcal{A}_P \begin{pmatrix} U_2 \\ \omega_1 \\ \omega_3 \end{pmatrix} = \begin{pmatrix} b_2 \\ b_4 \\ b_6 \end{pmatrix} - \mathcal{R}e \begin{pmatrix} c_2 \\ c_4 \\ c_6 \end{pmatrix} + \mathcal{G}a \mathcal{R}e \begin{pmatrix} \cos \theta \\ 0 \\ 0 \end{pmatrix} + \mathcal{O}_0(\mathcal{R}e^2), \tag{23}$$

where the additional terms come from the non-linearity of the Navier–Stokes equations. For any $i \in \{1, 2, \dots, 6\}$, they are given by

$$c_i = \int_{\Omega} (\mathbf{v}_S \cdot \nabla \mathbf{v}_S) \cdot \mathbf{v}^{(i)}. \tag{24}$$

Clearly, the corresponding solution (U_1, U_3, ω_2) to system (22) does not necessarily satisfy the conditions $U_1 = U_3 = 0$ required to obtain a steady solution. More precisely, the system (22) is equivalent to (using the fact that $\mathcal{A}_{55} \neq 0$):

$$\begin{cases} (A_{55}A_{11} - A_{15}^2)U_1 + (A_{55}A_{13} - A_{15}A_{35})U_3 \\ \quad = \mathcal{R}e (A_{15}c_5 - A_{55}c_1) + \mathcal{O}_0(\mathcal{R}e^2) \\ (A_{55}A_{13} - A_{15}A_{35})U_1 + (A_{55}A_{33} - A_{35}^2)U_3 \\ \quad = \mathcal{R}e (A_{35}c_5 - A_{55}(c_3 + \mathcal{G}a \sin \theta)) + \mathcal{O}_0(\mathcal{R}e^2) \\ A_{51}U_1 + A_{53}U_3 + A_{55}\omega_2 = -\mathcal{R}e c_5 + \mathcal{O}_0(\mathcal{R}e^2). \end{cases} \tag{25}$$

At first order with respect to the Reynolds number, the two first equations of this system write

$$\begin{cases} (A_{55}A_{11} - A_{15}^2)\tilde{U}_1 + (A_{55}A_{13} - A_{15}A_{35})\tilde{U}_3 = A_{15}c_5 - A_{55}c_1 \\ (A_{55}A_{13} - A_{15}A_{35})\tilde{U}_1 + (A_{55}A_{33} - A_{35}^2)\tilde{U}_3 \\ \quad = A_{35}c_5 - A_{55}(c_3 + \mathcal{G}a \sin \theta). \end{cases} \tag{26}$$

We can state now the following theorem.

Theorem 5.1. *We consider the solution $(\mathbf{v}, p, \mathbf{U}, \boldsymbol{\omega})$ to the system (4) associated to parameters (h, k) and to the Reynolds number $\mathcal{R}e$ (which is supposed to be small enough to have a unique solution). The asymptotic development of the velocity \mathbf{U} with respect to the Reynolds number takes the following form:*

$$\mathbf{U} = (0, U_2, 0) + \mathcal{R}e (\tilde{U}_1, \tilde{U}_2, \tilde{U}_3) + \mathcal{O}_0(\mathcal{R}e^2), \tag{27}$$

the components \tilde{U}_1 and \tilde{U}_3 being the solution of the linear system (26).

The linear system (26) can be written as $(\widetilde{U}_1, \widetilde{U}_3) = \mathcal{G}(h, k)$. The quantity $\mathcal{G}(h, k)$ represents, at first order in $\mathcal{R}e$ the components of the force exerted by the liquid in the directions orthogonal to the translational velocity of the disk (the lift).

Corollary 5.1. *The positions $(h, k) \in \omega$ of the ball providing steady solutions of (4) (at first order in $\mathcal{R}e$) correspond to the zeros of the vector field $\mathcal{G} : \omega \rightarrow \mathbb{R}^2$. More precisely, the current lines of this field are colinear with the projection of the ball trajectories to the plane $\mathcal{O}e_1e_3$.*

Remark 5.1. In the two dimensional situation, since $A_{55} = 0$, the condition to have a steady state solution reads $\widetilde{U}_3 = 0$, which is equivalent (at the first order) to the condition $c_3 = -\mathcal{G}a \sin \theta$. Such a condition can be viewed as

$$\mathcal{G}(h) = 0.$$

The objective of the remaining part of this work is to describe the strategy employed to numerically compute the vector field \mathcal{G} for channels of different sections ω .

6. Numerical applications

The aim of this section is to explain the implementation of the method proposed in the previous sections and to illustrate numerically the Segré-Silberberg effect [16] for cylinders having different sections ω . A similar study was done in a two-dimensional situation using a similar approach in [8].

6.1. Implementation of the method

In order to numerically implement the methodology described in the previous section we used several software. Firstly, for the description of the geometry of the half-domain Ω^+ and for the construction of a tetrahedral mesh of this domain, we employed Gmsh [9]. Particularly, we replace the infinite domain Ω^+ by a truncated domain in the direction e_2 : $\Omega_M^+ = \omega \times (0, M)$, see Remarks 3.1 and 3.4 for mathematical explanations. An example of the geometry and of a non-uniform mesh of such a domain are displayed in Fig. 3. The boundary conditions on the left extremity of the domain Ω_M^+ corresponding to $y = 0$ should be carefully tackled, taking into account the symmetry of the variables. Since we have to compute several integrals on the surface S of the ball, we consider non-uniform meshes which are much more refined on the surface of the ball B than on the lateral boundary of the cylinder.

For the numerical approximation of Stokes elementary problems (7), for the computation of the matrices \mathcal{A}_p and \mathcal{A}_l and for solving system (26), we used FreeFem++ [10]. More precisely, we numerically solve the weak formulations associated to these systems using P1b/P1 mixed finite elements combined with a pressure stabilization technique.

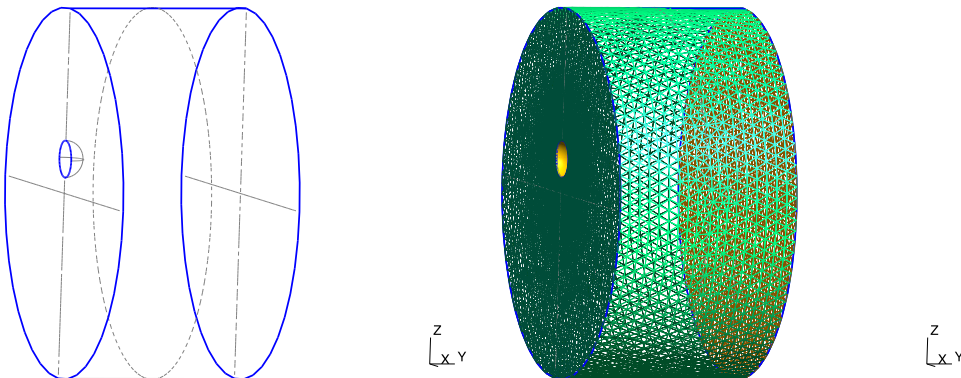


Fig. 3. The geometry and the mesh of domain $\Omega_{M=0.5}^+$ for a cylinder with circular section ω of radius $L = 0.5$, with a ball of radius $R = 0.05$ and of length $M = 0.5$.

For every geometrical situation considered, i.e. for every section ω and for every position (h, k) of the ball, we compute the solutions of system (25). Thus we obtain an approximation of the vector field \mathcal{G} provided by Corollary 5.1

6.2. Numerical illustrations

In this subsection we numerically illustrate the proposed method for different cross-sections ω . Firstly, we validate the method in the case of a cylinder with a circular section considering two directions for the gravity field. Secondly, we study the dynamic of a ball due to inertial forces in a cylinder with a rectangular section. Finally, we consider the situation reported in [13] in the context of particle separation using inertial focusing.

In what follows we compute the solution $(\widetilde{U}_1, \widetilde{U}_3)$ of the linear system (26) for different geometric configurations. Nevertheless, to simplify the notation, we drop the tilde on U_i and we denote by \mathcal{G} the vector field $\mathcal{G}(h, k)$.

6.2.1. Cylinder with circular cross-section

We consider cylinders with section ω being a disk of radius $L = 0.5$. The radius of the ball is set to $R = 0.05$ and the length of Ω_M^+ is chosen $M = 0.5$. Such a length seems to be sufficiently large such that the L^2 -norms of the traces of solutions of elementary problems (7) on the boundary $\omega \times \{M\}$ are close to the precision of the numerical scheme employed to solve these problems.

Gravity field perpendicular to the plane $\mathcal{O}e_1e_3$. First, we consider the situation where the gravity field and the vector e_2 are colinear, which is equivalent to take $\theta = 0$. Therefore, taking into account the symmetry of the disk, it is enough to take the center of the ball of coordinates $(h, k) = (0, z)$ with $z \in [0, L - \alpha R]$, where parameter $\alpha > 1$ is such that the ball does not touch the lateral wall of the cylinder. The first numerical experiment consists in computing the solution of system (25) for twenty such different positions of the ball. For each geometry we considered a non-uniform mesh with a characteristic size $c_5 = 0.0025$ on the surface of the ball and $c = 0.03$ on the lateral boundary. For example, one such mesh consists of a number of 164784 tetrahedra when the ball is positioned at the center of the cross section. In Fig. 4 we display the value of the component U_3 of the field \mathcal{G} which corresponds to the lift of the ball in the direction e_3 . Remark that the lift in the direction e_1 is zero and that $U_3(0, z) = -U_3(0, -z)$. The result illustrated in Fig. 4 is similar to the numerical results obtained in a two-dimensional framework in [8] and is in agreement with the experimental results in [14]. Concerning the positions of the ball for which steady solutions are obtained there is an unstable

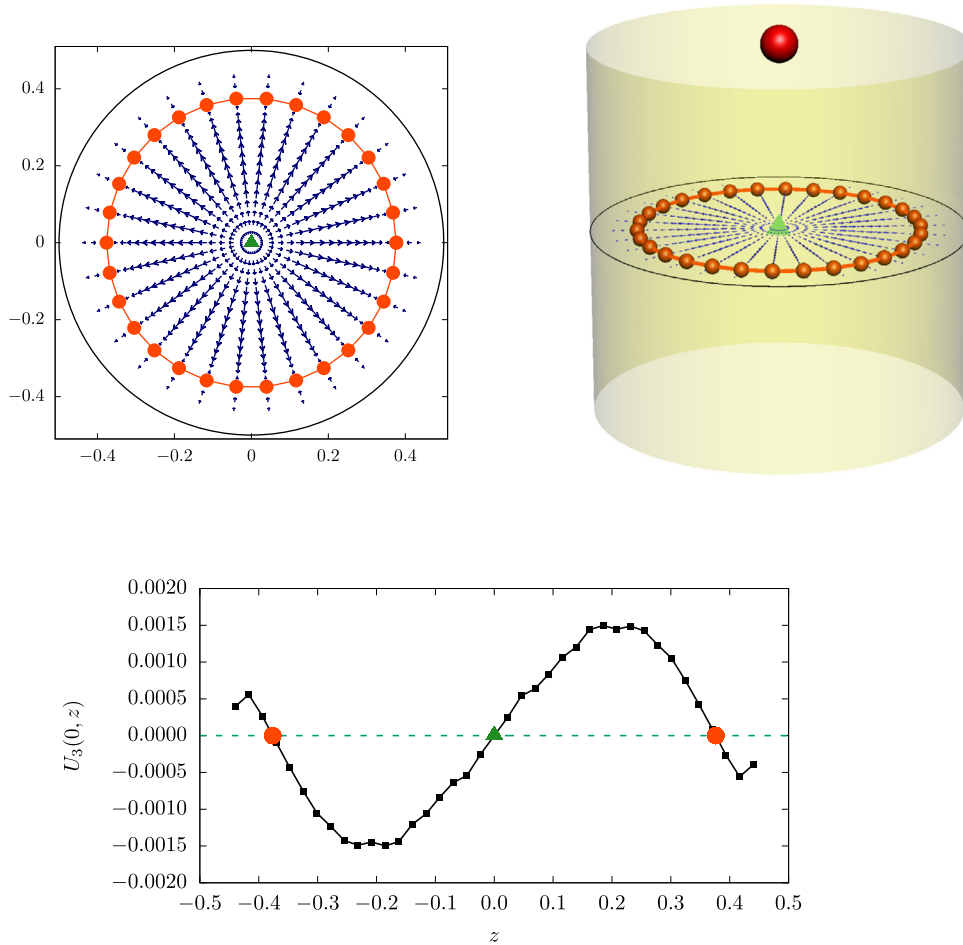


Fig. 4. Velocity U_3 of a ball situated at the position $(0, z)$ in a circular cylinder.

equilibrium in the center of the disk (\blacktriangle) and a circle having the same center as the disk ω of stable equilibria (\bullet).

In order to illustrate the convergence when the mesh size tends to zero, we consider the solution on a fine mesh with $c_S = 0.001$ and $c = 0.05$. On this fine mesh we compute a reference solution denoted $(U_1^r, U_3^r, \omega_2^r)$. We compare the solutions computed on six different levels of mesh (denoted $(U_1^i, U_3^i, \omega_2^i)$) obtained by taking $c = 0.05$ and $c_S \in \{0.002, 0.003, 0.004, 0.005, 0.006, 0.007\}$ to the reference solution. The results are displayed in Fig. 5. More precisely, we observe that the error $\|(U_1^i, U_3^i, \omega_2^i) - (U_1^r, U_3^r, \omega_2^r)\|$ decreases at a sub-linear order with respect to the characteristic size c_S . Since the numerical procedure combines numerical solving of partial differential equations and the resolution of a linear system with coefficients depending on integral and boundary integral of solutions of the partial differential equations, is difficult to obtain theoretical results concerning the order of the error.

Gravity colinear to the vector \mathbf{e}_3 . We set $\theta = \pi/2$, which corresponds to a gravity field with an opposite orientation with respect to the vector \mathbf{e}_3 . We consider a fluid of density $\rho_f = 10^3 \text{ kg} \cdot \text{m}^{-3}$ and solid balls of slightly higher density $\rho_s^1 = 1.05 \times 10^3 \text{ kg} \cdot \text{m}^{-3}$ and $\rho_s^2 = 1.1 \times 10^3 \text{ kg} \cdot \text{m}^{-3}$ respectively. Taking into account the symmetry of the disk and the orientation of \mathbf{g} , it is enough to take $(h, k) = (r \cos \beta, r \sin(\beta))$ with $r \in [0, L - \alpha R)$ and $\beta \in (-\frac{\pi}{2}, \frac{\pi}{2})$. We consider one hundred different positions of the ball of this form and we proceed as in the case where the gravity field was perpendicular to the plane Oe_1e_3 treated in the previous para-

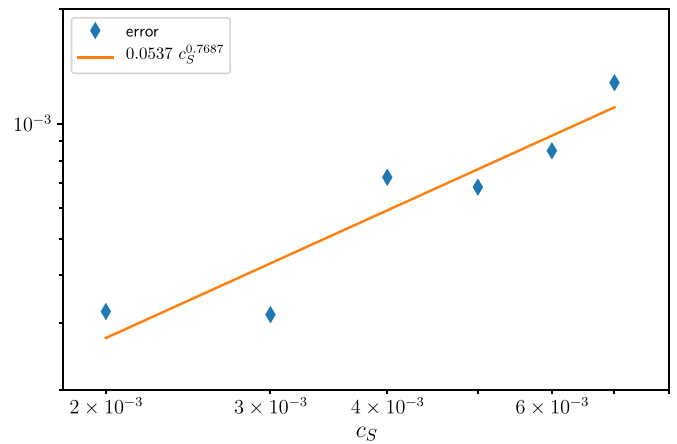


Fig. 5. Evolution of error $\|(U_1^i, U_3^i, \omega_2^i) - (U_1^r, U_3^r, \omega_2^r)\|$ with respect to c_S .

graph. In Fig. 6 (left) we display the field \mathcal{G} obtained for balls of density ρ_s^1 and in Fig. 6 (right) the corresponding results obtained for ρ_s^2 . We remark that the number of the equilibrium points changes with respect to ball's density. For ρ_s^1 there are three equilibrium positions all situated on the z -axis: one stable node (\bullet), one unstable node (\blacktriangle), and a saddle point (\blacklozenge). If the ball B has density ρ_s^2 there is only one stable equilibrium situated at the bottom of the z -axis. This behaviour is exactly the same as the one observed in a two-dimensional framework in [7].

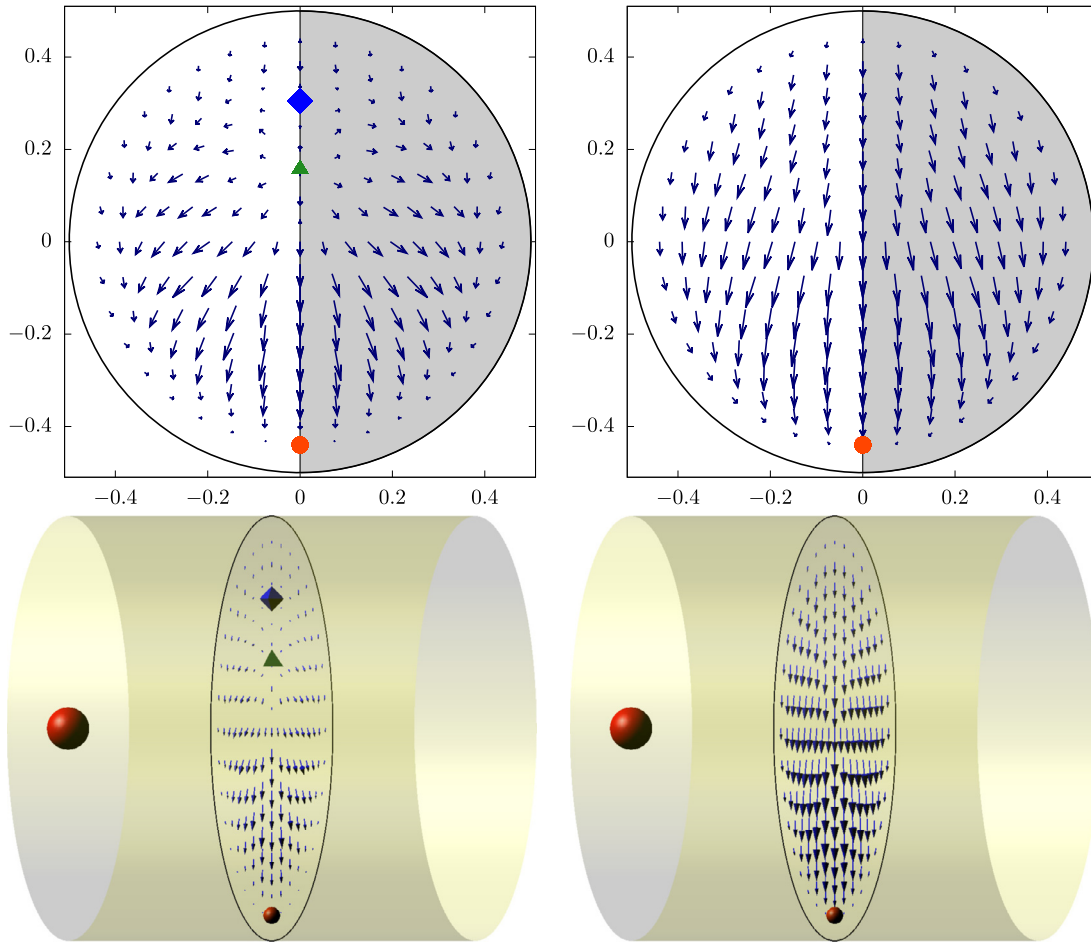


Fig. 6. Vector field \mathcal{G} in the case of cylinder with circular section and a gravity field corresponding to $\theta = \frac{\pi}{2}$, a fluid of density $\rho_f = 10^3 \text{ kg} \cdot \text{m}^{-3}$ and a ball of density $\rho_s^1 = 1.05 \times 10^3 \text{ kg} \cdot \text{m}^{-3}$ (left) and $\rho_s^2 = 1.1 \times 10^3 \text{ kg} \cdot \text{m}^{-3}$ (right).

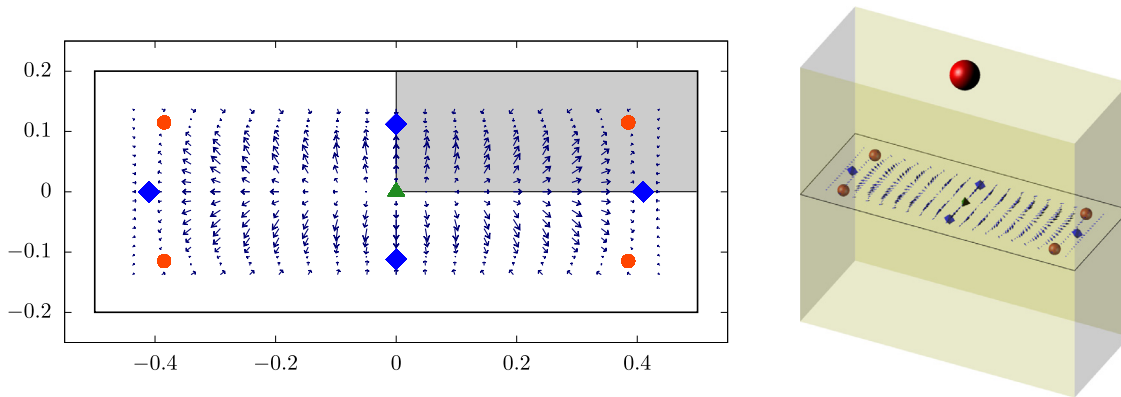


Fig. 7. Vector field \mathcal{G} in a case of a cylinder with rectangular section.

6.2.2. Cylinder with rectangular cross-section

We consider here the flow around balls B of radius $R = 0.05$ immersed in a fluid flowing inside a rectangular prism, or in other words, inside a cylinder of rectangular cross-section ω . The gravity field is oriented along the direction e_2 , i.e. $\theta = 0$. We take the cross-section of the rectangular prism to be the rectangle $\omega = (-\mathcal{L}, \mathcal{L}) \times (-\ell, \ell)$ with $\mathcal{L} = 0.5$ and $\ell = 0.2$. Taking into account the symmetry of the rectangle, it is enough to compute the solutions of system (25) for positions of the ball in the upper-right quarter of

ω , i.e., we consider $(h, k) \in \{(i\delta_1, j\delta_2) \text{ for } 0 \leq i, j \leq n\}$, $\delta_1 = (\mathcal{L} - \alpha R)/n$ and $\delta_2 = (\ell - \alpha R)/n$. Here, we have taken $\alpha = 1.25$. In Fig. 7 we represent the results obtained for this configuration. On the left-hand side we represent the field \mathcal{G} in ω obtained by symmetry from the field computed in a quarter of the domain (the gray rectangle) and the positions of the ball B which correspond to steady solutions. The same situation is represented in a three-dimensional view in the right-hand side of Fig. 7. To obtain some more information about the nature of these equilibrium positions we represent

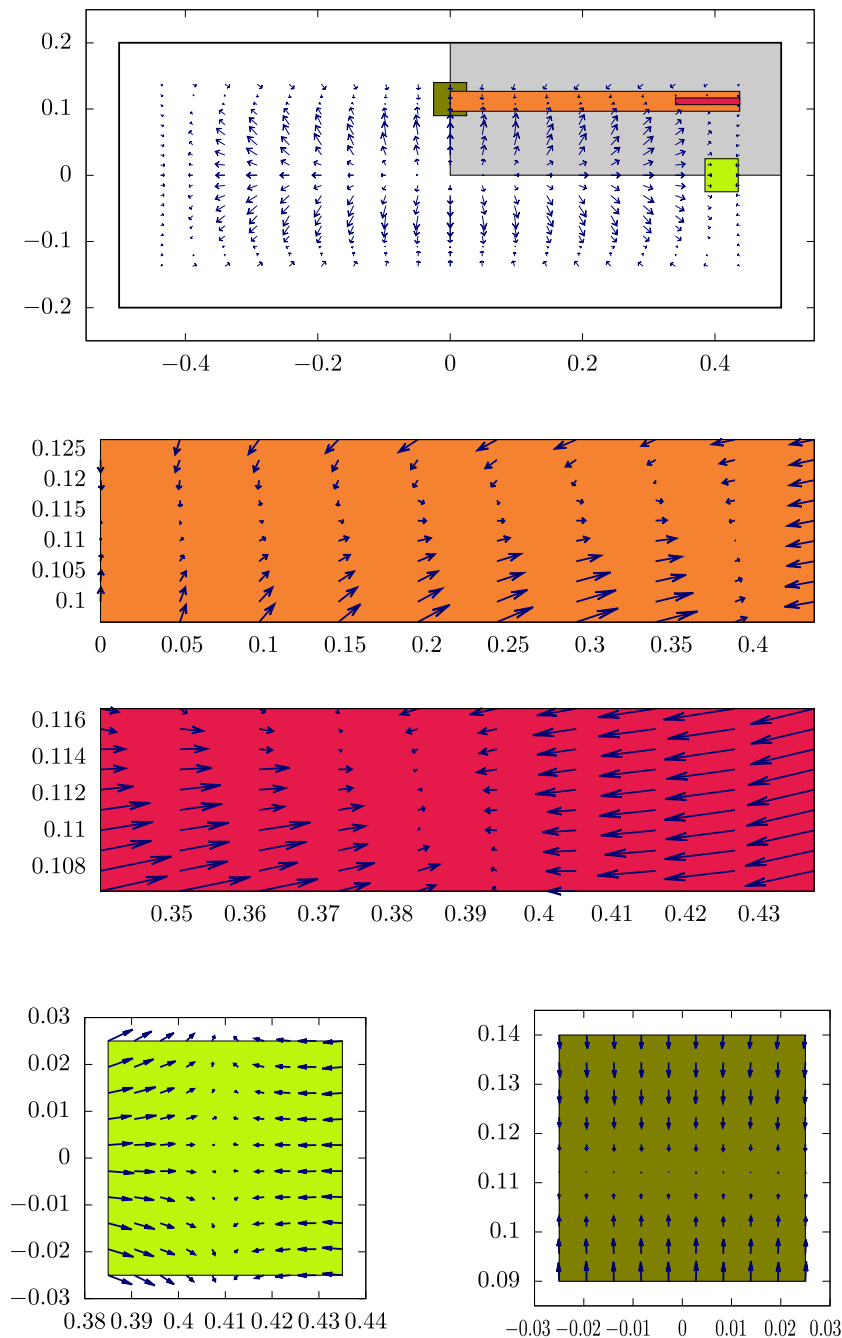


Fig. 8. Several zooms of the vector field \mathcal{G} in the case of a cylinder with rectangular section.

in Fig. 8 four different zooms around the points where the field \mathcal{G} is close to zero. It seems that there are nine such equilibrium positions:

- one unstable node (\blacktriangle)
- four saddle points near the middles of the edges (\blacklozenge)
- four stable nodes around the diagonals and near the corners of the rectangle (\bullet).

These results are in agreement with the results obtained in [2,3]. We mention that our method is not able to reproduce the behaviour observed in some other recent papers in microfluidics, where only two stable equilibria, situated near the middle of the longer edges of the rectangle are observed experimentally [12,17].

This is probably due to the fact that we approach the Navier-Stokes initial model by a first order development with respect to the Reynolds number and therefore our approach may be applied only for small enough Reynolds numbers.

6.2.3. Cylinder with triangular cross-section

In a recent article by Kim et al. [13] it was presented an application of the inertial migration for the separation of particles in suspension in a micro-fluid. The authors proposed an experimental setup consisting of several micro-channels of rectangular and triangular shapes in order to separate particles of different sizes being in suspension in a fluid.

In this last part, we consider the case of triangular shaped tubes. Let ω be an equilateral triangle of edge $L = 1$. Using the symmetry of this domain, it is enough to consider the sixth part of

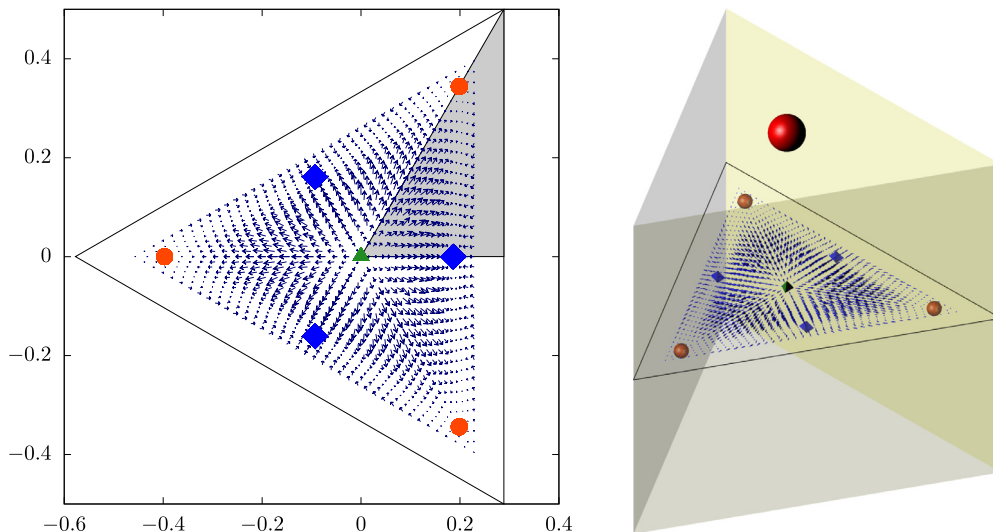


Fig. 9. Field \mathcal{G} and positions of the ball B for which steady solutions are obtained in the case where ω is an equilateral triangle.

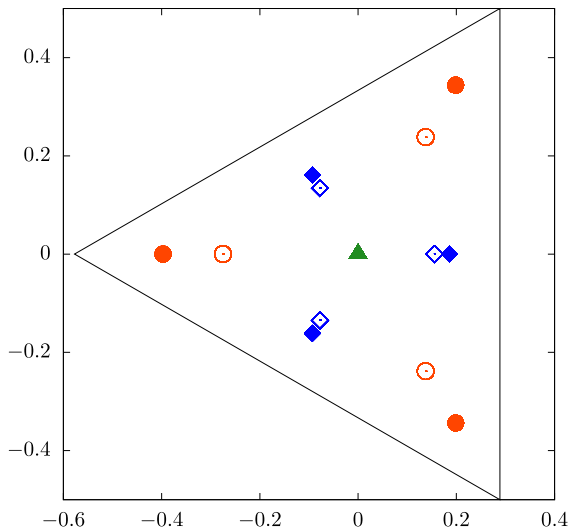


Fig. 10. Position of the ball for which steady solutions are obtained: filled shapes are obtained for a ball of radius $R = 0.05$ and empty shapes for $R = 0.1$.

this domain (triangle in gray in Fig. 9) for the positions of the ball. Nevertheless, we need to solve a number of 210 different geometric configurations in order to obtain the graphical representation in this figure.

There seem to be a number of seven positions for the ball B such that the corresponding field \mathcal{G} is zero. Among these positions, there is one unstable node near the mass center of the triangle (\blacktriangle), three saddle-points near the middle of each edge (\blacklozenge) and three stable nodes near the angles (\bullet). The results are in agreement with the results in [13] concerning the number of equilibrium points. As in the case of rectangles, due to the fact that our method is based on the approximation of the non-linear Navier-Stokes problem by linearizing at the first order with respect to the Reynolds number, we are probably not sufficiently close to the physical situations in a micro-channel to be able to seize the behavior described in [13].

In fact, for the applications to particle separations it is important that for balls of different sizes have different positions (h, k) providing steady solutions. In Fig. 10 we represent the positions for

which we obtain steady solutions for balls of radius $R = 0.05$ (\blacktriangle , \blacklozenge , \bullet) and for balls of radius $R = 0.1$ (the corresponding unfilled shapes). We therefore observe that bigger particles have focusing positions situated closer to the center of the channel than smaller particles.

7. Conclusion

The main contribution of this work is the generalization of the method proposed in [8] to the three-dimensional case. More precisely, we reduce the computation of the inertial velocity of a solid particle immersed in a fluid flowing in a three-dimensional pipe to a problem having the same structure as the one in [8]. A finely tuned computational strategy was implemented in order to tackle the practical difficulties related to the geometry of the problem and to the high computational costs. The finite elements method was employed to approach the fluid-structure system on a mesh which, using the symmetry of the problem, discretizes only half of the pipe, and which is much finer on the spherical particle than on the pipe's walls. The proposed method was validated on the well known situation of inertial migration of spherical particles in a cylinder with circular section and illustrated on other less symmetric geometries as cylinder with triangular and rectangular cross-sections. For all the considered geometries we discuss the number and the nature of the equilibrium positions, this information being important for applications as separation of micro-particles of different sizes.

Several developments and generalizations of this method are possible. From a theoretic point of view, it will be interesting to approach the initial nonlinear fluid-structure by a development with respect to the Reynolds number at an order higher than one. In this way, the non-linearity of the system could be treated in a more precise manner. Another possible extension is to consider more complex geometries: what happens if the cylinder is torsioned, if the particle is not spherical or if there are more than one particle?

References

- [1] Asmolov ES. The inertial lift on a spherical particle in a plane poiseuille flow at large channel Reynolds number. *J Fluid Mech* 1999;381:63–87.
- [2] Bhagat AAS, Kuntaegowdanahalli SS, Papautsky I. Enhanced particle filtration in straight microchannels using shear-modulated inertial migration. *Phys Fluids* 2008;20(10):101702.

- [3] Chun B, Ladd AJC. Inertial migration of neutrally buoyant particles in a square duct: an investigation of multiple equilibrium positions. *Phys Fluids* 2006;18(3):031704.
- [4] Carlo DD, Edd JF, Humphry KJ, Stone HA, Toner M. Particle segregation and dynamics in confined flows. *Phys Rev Lett* 2009;102(9):094503.
- [5] Feng J, Hu HH, Joseph DD. Direct simulation of initial value problems for the motion of solid bodies in a Newtonian fluid part 1. sedimentation. *J Fluid Mech* 1994;261:95–134.
- [6] Galdi G. An introduction to the mathematical theory of the Navier-Stokes equations: nonlinear steady problems, 39. Springer Tracts in Natural Philosophy; 1998.
- [7] Galdi GP. Mathematical problems in classical and non-newtonian fluid mechanics. In: Hemodynamical flows. Springer; 2008. p. 121–273.
- [8] Galdi GP, Heuveline V. Lift and sedimentation of particles in the flow of a viscoelastic liquid in a channel. In: Free and moving boundaries, volume 252 of Lect. Notes Pure Appl. Math., Boca Raton, FL: Chapman & Hall/CRC; 2007. p. 75–110.
- [9] Geuzaine C, Remacle J-F. Gmsh: a 3-d finite element mesh generator with built-in pre- and post-processing facilities. *Int J Numer Methods Eng* 2009;79(11):1309–31.
- [10] Hecht F. New development in freefem++. *J Numer Math* 2012;20(3–4):251–65.
- [11] Johnson AA, Tezduyar TE. Simulation of multiple spheres falling in a liquid-filled tube. *Comput Methods Appl Mech Eng* 1996;134(3–4):351–73.
- [12] Kim J-A, Lee J, Wu C, Nam S, Carlo DD, Lee W. Inertial focusing in non-rectangular cross-section microchannels and manipulation of accessible focusing positions. *Lab Chip* 2016;16(6):992–1001.
- [13] Kim J-a, Lee J-R, Je T-J, Jeon E-c, Lee W. Size-dependent inertial focusing position shift and particle separations in triangular microchannels. *Anal Chem* 2018;90(3):1827–35.
- [14] Matas J-P, Morris JF, Guazzelli E. Inertial migration of rigid spherical particles in poiseuille flow. *J Fluid Mech* 2004;515:171–95.
- [15] Schonberg JA, Hinch EJ. Inertial migration of a sphere in poiseuille flow. *J Fluid Mech* 1989;203:517–24.
- [16] Segré G, Silberberg AJ. Behaviour of macroscopic rigid spheres in poiseuille flow part 2. experimental results and interpretation. *J Fluid Mech* 1962;14(1):136–57.
- [17] Zhou J, Papautsky I. Fundamentals of inertial focusing in microchannels. *Lab Chip* 2013;13(6):1121–32.